Atoms **2015**, *3*, 273-298; doi: 10.3390/atoms3030273

OPEN ACCESS

atoms

ISSN 2218-2004
www.mdpi.com/journal/atoms

Article

Spectra of W VIII and W IX in the EUV Region

Alexander Ryabtsev [1,*], Edward Kononov [1,†], Rimma Kildiyarova [1,†], Wan-Ü Lydia Tchang-Brillet [2,†], Jean-Francois Wyart [2,3,†], Norbert Champion [2,†] and Christophe Blaess [2,†]

[1] Institute of Spectroscopy, Russian Academy of Sciences, Troitsk, Moscow 142190, Russia; E-Mails: kononov@isan.troitsk.ru (E.K.); rimma@isan.troitsk.ru (R.K.)

[2] LERMA, Observatoire de Paris-Meudon, PSL Research University, UMR8112 du CNRS, Sorbonne Universités, UPMC Univ. Paris 06, 92195 Meudon, France; E-Mails: lydia.tchang-brillet@obspm.fr (W.U.L.T.-B.); norbert.champion@obspm.fr (N.C.); christophe.blaess@obspm.fr (C.B.)

[3] Laboratoire Aimé Cotton, CNRS UMR9188, Université Paris-Sud, ENS Cachan, Bâtiment 505, F-91405 Orsay Cedex, France; E-Mail: Jean-Francois.Wyart@lac.u-psud.fr

† These authors contributed equally to this work.

* Author to whom correspondence should be addressed; E-Mail: ryabtsev@isan.troitsk.ru; Tel.: +7-495-851-0225.

Academic Editor: Bastiaan J. Braams

Received: 8 April 2015 / Accepted: 15 June 2015 / Published: 30 June 2015

Abstract: The results obtained on the W VIII spectrum as well as on the isoelectronic spectra Lu V, Hf VI, Ta VII, and Re IX in the VUV wavelength region are summarized with emphasis on the main trends along the isoelectronic sequence. A total of 187 lines of W VIII in the region of 160–271 Å were accurately measured and identified, 98 levels were found, and transition probabilities calculated. The isoelectronic regularities support the data on W VIII. A list of spectral lines in the region of 170–199 Å, considered as belonging to W IX, is presented.

Keywords: atomic data for tungsten; vacuum ultraviolet; ion spectra; wavelengths; energy levels; transition probabilities; parametric calculations

---

1. Introduction

One of the key components of the international tokamak ITER, the divertor, is planned to be made from refractory tungsten. Tungsten sputtered from the divertor target plates will be transported to the plasma core where it contributes to radiative losses. The plasma parameters that are expected in the divertor will lead to excitation of tungsten ions up to approximately the 15th stage of ionization [1]. It is thus important to know the influx of tungsten. Emission lines from tungsten ions provide a diagnostic tool to solve this problem. However, as was shown in the compilation by Kramida and Shirai in 2009 [2] and the subsequent update [3], experimental data on classified line wavelengths and on energy levels were available only for the ions up to the sixth ionization stage. The W VIII–W XXVII spectra had never been analysed before.

An emission spectrum from a tokamak was recorded [4] in 1996 where the tungsten was injected by a blow-off method as an impurity in the plasma of the tokamak. The spectrum was taken with a low resolution of 5 Å and two broad peaks around 190 and 230 Å were tentatively assigned to radiations from the W^{7+} ion (W VIII). It was even uncertain to which configuration the ground state of this ion belongs. The authors of the compilation [2], based on the analysis of the $4f^{13}5s^25p^6ns$ and $4f^{14}5s^25p^5(^2P_{3/2})ns$ series of W VII by Sugar and Kaufman [5], asserted that the ground state of W VIII is probably $4f^{13}5s^25p^6$ $F_{7/2}$, whereas $4f^{14}5s^25p^5$ $^2P_{3/2}$ is located 800 ± 700 cm^{-1} above it. They also estimated the fine structure splitting of $4f^{13}5s^25p^6$ $^2F_{7/2}$-$^2F_{5/2}$ to be 17440 ± 60 cm^{-1}. More recently, a tungsten spectrum excited in a spheromak and recorded in the range of 180–450 Å with a resolution of 0.3 Å was published [6]. Along with 10 known W VI–W VII lines, an incompletely resolved structure was observed for the tungsten lines with maxima at about 200 and 250 Å; 17 peaks of this structure were attributed to the transitions in W VI–W VIII. However, the low resolution of the instruments used in both experimental studies [5,6] did not allow any reliable interpretation of the W VIII spectrum. Except for the calculations showing the position of W IX resonance transitions [7], there was no other information on the W IX spectrum.

To extend the data on tungsten ions needed for fusion plasma modeling, we undertook an investigation of the W VIII and W IX spectra. Given the complexity of these spectra, it was relevant to perform a systematic study of neighboring isoelectronic spectra making use of possible isoelectronic regularities. The present project "Spectra of W VIII and W IX and Isoelectronic Ions of Hf, Ta and Re" has been carried out within the framework of the IAEA Coordination Research Project (CRP) entitled "Spectroscopic and Collisional Data for Tungsten from 1 eV to 20 keV" [8]. An extensive analysis of the W VIII spectrum was published [9,10], followed by the analyses of the isoelectronic Hf VI [11], Ta VII [12], and Re IX [13]. In this paper, we will summarize our results obtained on W VIII and its isoelectronic spectra [9–13] with an emphasis on the main trends along the isoelectronic sequence. Preliminary results on the W IX spectrum will be reported and discussed.

2. Experimental Techniques

For all studied isoeletronic spectra with the W VIII (Hf, Ta, Re), two complementary experimental settings were used.

At the Institute of Spectroscopy in Troitsk, the spectra were recorded in the region 130–350 Å on a 3-m grazing incidence spectrograph equipped with a 3600 lines/mm, gold-coated holographic grating. The spectra were excited in a three-electrode, low-inductance vacuum spark with the peak current varied in the range of 9–50 kA. The spectra were recorded on Kodak SWR photographic plates and FUJI Imaging Plate BAS-TR2025. The photographic plate spectra were measured on an Epson Expression 1000 XL scanner. The observed wavelength resolution was about 0.015 Å. The anode was made of the appropriate element rod, whereas titanium was used for the cathode. Wavelengths were calibrated using titanium ion lines [14] as standards with the estimated uncertainty of the measured wavelengths ± 0.005 Å.

The spectra recorded on the FUJI Imaging Plate were scanned with a Typhoon FLA 9500 reader using a 10 µm sample step. Produced images were processed and analysed with ImageQuant TL 7.0 image analysis software, giving a digitized spectrum by signal integration along spectrum lines. This spectrum was further reduced using the program GFit [15], resulting in a table of line centres and intensities. The wavelength resolution in the case of image plates was about 0.03 Å, keeping in mind the 25 µm optical resolution of the Typhoon FLA 9500 reader. Therefore, these spectra were used for the intensity measurement, taking advantage of the linear intensity response of the image plate. It should be noticed that the wavelength dependence of the spectrograph efficiencies and image plate sensitivity were not taken into account.

At the Meudon Observatory, a similar but different triggered spark source was used to produce emission spectra. Spectra were recorded on a 10 m normal incidence spectrograph. This instrument is equipped with a 3600 lines/mm concave grating, resulting in a plate factor of ~0.25 Å/mm in the first order and a resolution of 0.008Å with a slit width of 30 µm in the range of 200–3000 Å. In the present work at the Meudon Observatory, spectra were recorded in the region of 180–500 Å on phosphor image plates (Fuji BAS-TR 2040), which were processed by a specific reader as described in a previous work on Nd V [16]. A Perkin-Elmer CYCLONE reader with a 43 µm sample step had been used in some earlier recordings, and more recent recordings were read using a FUJI FLA 9000 reader with a 10 µm sample step. In the last case, the high resolution of 0.008 Å of the spectrograph was preserved.

Well exposed spectra were obtained down to 180 Å on this normal incidence instrument, which provides an overlapping wavelength range with the grazing incidence instrument at Troitsk. A comparison of line intensities in the region of the overlap was helpful in selecting lines belonging to the spectrum under study.

Line identifications were made with the aid of the program IDEN [17]. IDEN uses an experimental spectrum, calculated energy levels, and transition probabilities. *Ab initio* calculations were performed by the Hartree–Fock method with relativistic corrections (HFR) with the use of the RCN-RCN2-RCG chain of the Cowan codes [18]. The derivation of radial energy parameters that leads to minimal deviations between experimental and theoretical energies, and optimal eigenfunctions, was performed with the last code RCE of the Cowan package [18].

The level energies derived from the line identifications were optimized by using the least-squares program LOPT [19].

3. Results and Discussion

3.1. W VIII and Isoelectronic Ion Spectra

According to *ab initio* calculations with the Cowan code [18], the spectrum of the resonance transitions of W VIII is expected to be formed by the decays from the interacting $4f^{12}5s^25p^65d$ + $4f^{13}5s^25p^5(5d+6s)$ + $4f^{14}5s^25p^4(5d+6s)$ + $4f^{14}5s5p^6$ excited configurations of the even parity to the $4f^{13}5s^25p^6$ and $4f^{14}5s^25p^5$ odd parity configurations. For better prediction of the spectrum, the *ab initio* calculations had to be properly scaled. Usually, the scaling factors are estimated by extrapolation along an isoelectronic sequence. However, of all these even configurations, only $4f^{12}5s^25p^65d$ was studied in the isoelectronic sequence of W VIII, the last spectrum being Lu V [20]. No other even configuration was known in any of the ions of the sequence, nor was the $4f^{14}5s^25p^5$ odd parity configuration observed in this isoelectronic sequence. Therefore, a study of the isoelectronic spectra of the neighbouring chemical elements with the aim of finding these unknown configurations was necessary for reliable identifications in the W VIII spectrum.

Figure 1 shows the positions of low-lying configurations relative to the $4f^{13}5s^25p^6$ configuration in the sequence Lu V–Re IX according to the Hartree-Fock calculations. It is seen that the configurations of both parities cross along the sequence, W VIII being the most intricate case.

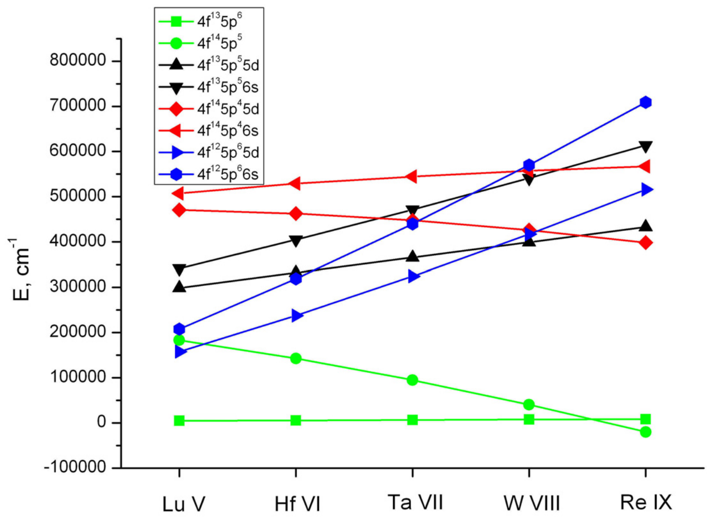

Figure 1. Calculated average energies of the low-lying configurations in the W VIII isoelectronic sequence.

The structure of the energy levels in Hf VI–Re IX spectra is shown in Figure 2. Red bars mark experimentally found levels. Grey bars correspond to the calculated positions of unknown levels. Dashed vertical lines divide two systems formed by excitation of one electron from one of the two lowest configurations $4f^{14}5s^25p^5$ and $4f^{13}5s^25p^6$. Electric dipole (E1) transitions are possible inside these two systems. There is also one intersystem E1 transition array connecting levels from the two systems: $4f^{14}5s^25p^5$–$4f^{13}5s^25p^55d$. The general trend along the isoelectronic sequence is that the configurations formed by an excitation from the $5p^5$ subshell of the $4f^{14}5s^25p^5$ configuration move down and the $4f^{12}5s^25p^6(5d+6s)$ configurations move up relative to the $4f^{13}5s^25p^5(5d+6s)$ configurations as the ion change increases. Because of the large spread of the even configurations, they overlap to some extent in all ions, depending on the change of relative positions along the isoelectronic sequence. The configuration interactions lead to a mixture of their wave functions, resulting in the observations of different electric dipole forbidden transitions. These transitions contribute to establishing the connection between the levels of two excitation systems with higher reliability. It is visible from Figure 2 that we found the levels in all but the $4f^{14}5s5p^6$ excited configurations of the even parity that decay to the low-lying odd $4f^{14}5s^25p^5$ and $4f^{13}5s^25p^6$ configurations. The $4f^{12}5s^25p^66s$ configuration is metastable. It does not decay down by E1 transitions. However, due to configuration interactions, transitions from this configuration were detected and they helped to establish some of its levels in Ta VII. Below, we discuss some individual features of the studied spectra.

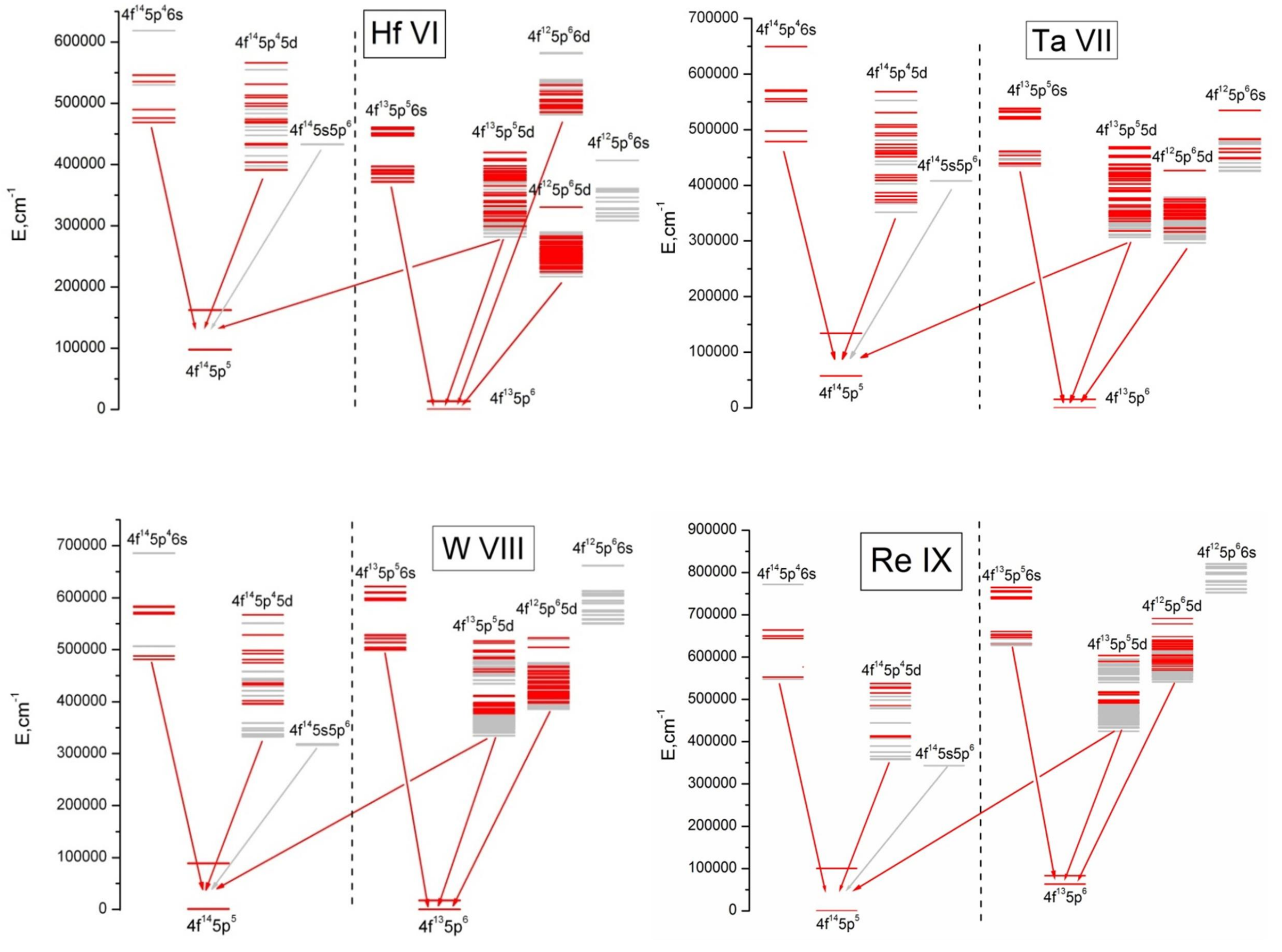

Figure 2. Energy levels of low-lying configurations of Hf VI, Ta VII, W VIII, and Re IX. Red horizontal bars show levels established in this work. Calculated positions of unknown levels are shown in grey colour. Dashed vertical lines divide systems formed by excitation of the two lowest configurations $4f^{14}5s^25p^5$ and $4f^{13}5s^25p^6$ (the subshell $5s^2$ is omitted from the configuration names except for $4f^{14}5s5p^6$). Arrows indicate electron dipole transitions between the configurations.

W VIII [9,10]. Figure 3 shows an experimental spectrum of tungsten excited in a vacuum spark source from Troitsk, with a peak current of 50 kA. Our spectrum reproduced, with a resolution an order of magnitude higher, the entire structure in the regions 200 and 250 Å, as well as the individual peaks of tungsten emission in other regions, which were detected in the spheromak spectrum [6]. Because of the large spin-orbit splitting of the 5p electron, the spectrum of W VIII is roughly divided into three groups located approximately at 170, 200, and 250 Å. The lines around 170 Å are identified with the $4f^{13}5s^25p^6$–$4f^{13}5s^25p^5{}_{j=1/2}6s$ and $4f^{14}5s^25p^5$–$4f^{14}5s^25p^46s$ transitions. The lines of the group at 200 Å are mostly identified as the $4f^{13}5s^25p^6$– ($4f^{13}5s^25p^5{}_{j=1/2}5d$ + $4f^{13}5s^25p^5{}_{j=3/2}6s$) transitions, contrary to a former suggestion [6] that they could belong to transitions from the $4f^{14}5s^25p^45d$ configuration. Intense lines in the 250 Å region belong mostly to the $4f^{13}5s^25p^6$–$4f^{13}5s^25p^5{}_{j=3/2}5d$ transitions.

The list of 187 identified W VIII lines is presented in Table 1. It also contains the products gA of the upper level statistical weight and the transition probability per unit time (Einstein coefficient A) and the energies of the lower and the upper levels of the transitions, respectively. The transition probabilities were calculated with wavefunctions obtained by Cowan's code with optimised energy parameters. The wavefunctions show mixtures of states within the same configuration, as well as mixtures of states belonging to different interacting configurations. Therefore, in Table 1, the upper levels of the transitions are designated by their energies and their J-values, whereas for convenience, a configuration name is given according to the output files from Cowan's code in spite of possible ambiguity in some cases.

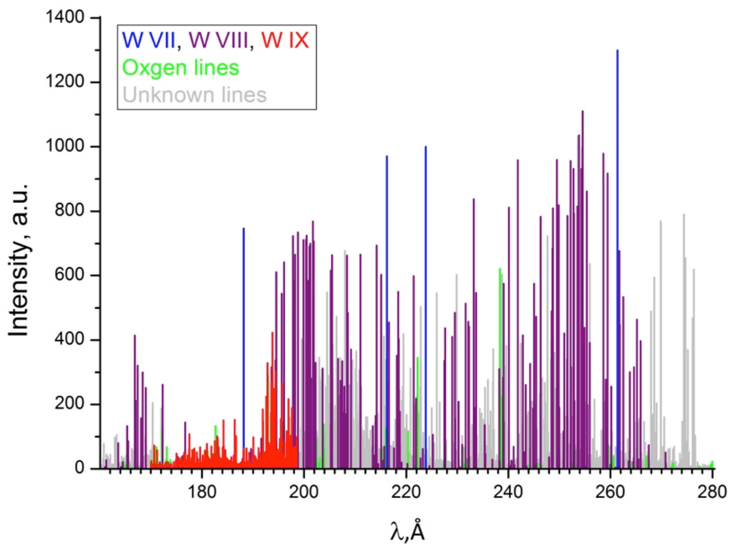

Figure 3. Spectrum of tungsten excited in a vacuum spark with the peak current 50 kA with identification of the lines.

It was firmly established that the ground state of W VIII is $4f^{13}5s^25p^6\ {}^2F_{7/2}$. A splitting of 17410 ± 5 cm^{-1} for the $4f^{13}5s^25p^6\ {}^2F$ term was found in close agreement with the predicted [2] value 17440 ± 60 cm^{-1}. The $4f^{14}5s^25p^5\ {}^2P_{3/2}$ level was found to be located 1231 ± 3 cm^{-1} above the ground state, again in agreement with the predicted value 800 ± 700 cm^{-1} [2,5]. The ${}^2P_{3/2}$–${}^2P_{1/2}$ interval was derived as 87890 ± 6 cm^{-1}, slightly different from the predicted [2] value 87100 ± 300 cm^{-1}. Overall, 97 levels of the excited configurations were located.

Table 1. Identified lines in the spectrum of W VIII.

λ (Å)[h]	o-c[a] (Å)	σ (cm^{-1})	Int.	gA ($10^8 \cdot s^{-1}$)	Lower Level			Upper Level		
					Config.[b]	Term	E (cm^{-1})	Config.[c]	J	E(cm^{-1})
160.940	−0.002	621351	5	10	$4f^{13}5p^6$	$^2F_{7/2}$	0	$4f^{13}5p^56s$	5/2	621343
161.057	−0.002	620897	4	10	$4f^{14}5p^5$	$^2P_{3/2}$	1233	$4f^{13}5p^56s$	3/2	622123
161.260	−0.002	620118	27	147	$4f^{14}5p^5$	$^2P_{3/2}$	1233	$4f^{13}5p^56s$	5/2	621343
163.596	0.006	611261	80	12	$4f^{13}5p^6$	$^2F_{7/2}$	0	$4f^{13}5p^56s$	7/2	611283
164.143	−0.005	609225	6	4	$4f^{13}5p^6$	$^2F_{7/2}$	0	$4f^{13}5p^56s$	5/2	609206
164.479	−0.002	607979	21	1	$4f^{14}5p^5$	$^2P_{3/2}$	1233	$4f^{13}5p^56s$	5/2	609206
165.369	0.001	604708	130	1365	$4f^{13}5p^6$	$^2F_{5/2}$	17410	$4f^{13}5p^56s$	3/2	622123
165.583	0.002	603927	86	900	$4f^{13}5p^6$	$^2F_{5/2}$	17410	$4f^{13}5p^56s$	5/2	621343
166.827	0.000	599422	410	3397	$4f^{13}5p^6$	$^2F_{7/2}$	0	$4f^{13}5p^56s$	9/2	599423
166.971	−0.001	598905	210	1373	$4f^{13}5p^6$	$^2F_{7/2}$	0	$4f^{13}5p^56s$	7/2	598904
167.382		597435	320	2172	$4f^{13}5p^6$	$^2F_{7/2}$	0	$4f^{13}5p^56s$	5/2	597436
168.084		594941	160	649	$4f^{13}5p^6$	$^2F_{7/2}$	0	$4f^{13}5p^56s$	7/2	594941
168.381	−0.005	593891	300	2578	$4f^{13}5p^6$	$^2F_{5/2}$	17410	$4f^{13}5p^56s$	7/2	611283
168.980	0.003	591787	250	584	$4f^{13}5p^6$	$^2F_{5/2}$	17410	$4f^{13}5p^56s$	5/2	609206
171.727	0.002	582320	21	347	$4f^{14}5p^5$	$^2P_{3/2}$	1233	$4f^{14}5p^46s$	3/2	583560
171.973	0.002	581488	8	46	$4f^{13}5p^6$	$^2F_{5/2}$	17410	$4f^{13}5p^56s$	7/2	598904
172.295	0.001	580400	260	1431	$4f^{14}5p^5$	$^2P_{3/2}$	1233	$4f^{14}5p^46s$	5/2	581635
175.199	−0.003	570781	38	561	$4f^{14}5p^5$	$^2P_{3/2}$	1233	$4f^{14}5p^46s$	1/2	572004
176.237	−0.002	567418	40	299	$4f^{14}5p^5$	$^2P_{3/2}$	1233	$4f^{14}5p^46s$	3/2	568644
176.630	−0.002	566156	54	111	$4f^{13}5p^6$	$^2F_{5/2}$	17410	$4f^{14}5p^46s$	3/2	583560
176.694	0.002	565951	150	405	$4f^{14}5p^5$	$^2P_{3/2}$	1233	$4f^{14}5p^46s$	3/2	567191
177.232	−0.002	564232	23	90	$4f^{13}5p^6$	$^2F_{5/2}$	17410	$4f^{14}5p^46s$	5/2	581635
181.410	−0.001	551237	17	202	$4f^{13}5p^6$	$^2F_{5/2}$	17410	$4f^{14}5p^46s$	3/2	568644
181.888	−0.003	549788	12	419	$4f^{13}5p^6$	$^2F_{5/2}$	17410	$4f^{14}5p^46s$	3/2	567191
187.608	−0.009	533027	12	56	$4f^{14}5p^5$	$^2P_{1/2}$	89123	$4f^{13}5p^56s$	3/2	622123
189.616	−0.002	527381	62	130	$4f^{13}5p^6$	$^2F_{7/2}$	0	$4f^{13}5p^56s$	7/2	527376
189.667	−0.004	527241	58	718	$4f^{14}5p^5$	$^2P_{3/2}$	1233	$4f^{14}5p^45d$	1/2	528462
191.348[e]	0.001	522607	11	1069	$4f^{13}5p^6$	$^2F_{7/2}$	0	$4f^{12}5p^65d$	5/2	522610
191.617	0.001	521875	94	95	$4f^{13}5p^6$	$^2F_{7/2}$	0	$4f^{13}5p^56s$	5/2	521876
192.070	0.000	520643	32	3	$4f^{14}5p^5$	$^2P_{3/2}$	1233	$4f^{13}5p^56s$	5/2	521876
193.614	0.001	516492	320	102	$4f^{13}5p^6$	$^2F_{7/2}$	0	$4f^{13}5p^55d$	5/2	516493
194.077	0.000	515259	61	77	$4f^{14}5p^5$	$^2P_{3/2}$	1233	$4f^{13}5p^55d$	5/2	516493
194.315	0.000	514628	52	59	$4f^{13}5p^6$	$^2F_{7/2}$	0	$4f^{13}5p^56s$	5/2	514628
194.397	0.001	514411	340	249	$4f^{13}5p^6$	$^2F_{7/2}$	0	$4f^{13}5p^56s$	7/2	514413
194.527	−0.002	514068	610	2278	$4f^{13}5p^6$	$^2F_{7/2}$	0	$4f^{13}5p^56s$	5/2	514063
194.998	0.002	512825	47	57	$4f^{14}5p^5$	$^2P_{3/2}$	1233	$4f^{13}5p^56s$	5/2	514063
195.021	0.009	512765	16	251	$4f^{13}5p^6$	$^2F_{7/2}$	0	$4f^{13}5p^55d$	7/2	512790
195.598	−0.004	511252	540	2166	$4f^{13}5p^6$	$^2F_{5/2}$	17410	$4f^{13}5p^56s$	3/2	528652
196.093	0.002	509961	640	2868	$4f^{13}5p^6$	$^2F_{5/2}$	17410	$4f^{13}5p^56s$	7/2	527376
197.835	0.000	505472	720	8923	$4f^{13}5p^6$	$^2F_{5/2}$	17410	$4f^{12}5p^65d$	3/2	522881
197.941[e]	0.000	505202	410	1569	$4f^{13}5p^6$	$^2F_{5/2}$	17410	$4f^{12}5p^65d$	5/2	522610

Table 1. *Cont.*

λ (Å)[h]	o-c[a] (Å)	σ (cm^{-1})	Int.	gA ($10^8 \cdot s^{-1}$)	Lower Level			Upper Level		
					Config.[b]	Term	E (cm^{-1})	Config.[c]	J	E(cm^{-1})
198.171		504613	590	5013	$4f^{13}5p^6$	$^2F_{7/2}$	0	$4f^{13}5p^56s$	9/2	504615
198.229	0.000	504467	670	3950	$4f^{13}5p^6$	$^2F_{5/2}$	17410	$4f^{13}5p^56s$	5/2	521876
198.625	−0.001	503461	16	5	$4f^{14}5p^5$	$^2P_{3/2}$	1233	$4f^{12}5p^65d$	3/2	504691
198.779		503070	740	5840	$4f^{13}5p^6$	$^2F_{7/2}$	0	$4f^{13}5p^56s$	7/2	503071
199.875		500312	710	1958	$4f^{13}5p^6$	$^2F_{7/2}$	0	$4f^{13}5p^56s$	5/2	500313
200.367	0.000	499085	710	18664	$4f^{13}5p^6$	$^2F_{5/2}$	17410	$4f^{13}5p^55d$	5/2	516493
200.483	−0.001	498796	730	30107	$4f^{13}5p^6$	$^2F_{7/2}$	0	$4f^{13}5p^55d$	7/2	498792
200.787	−0.001	498041	580	20835	$4f^{13}5p^6$	$^2F_{7/2}$	0	$4f^{13}5p^55d$	5/2	498037
201.079	−0.004	497317	690	2027	$4f^{14}5p^5$	$^2P_{3/2}$	1233	$4f^{14}5p^45d$	3/2	498541
201.119	0.000	497217	440	3154	$4f^{13}5p^6$	$^2F_{5/2}$	17410	$4f^{13}5p^56s$	5/2	514628
201.205	−0.001	497006	700	1388	$4f^{13}5p^6$	$^2F_{5/2}$	17410	$4f^{13}5p^56s$	7/2	514413
201.288	0.001	496800	280	2238	$4f^{14}5p^5$	$^2P_{3/2}$	1233	$4f^{13}5p^55d$	5/2	498037
201.739		495691	770	38110	$4f^{13}5p^6$	$^2F_{7/2}$	0	$4f^{13}5p^55d$	9/2	495690
201.864	−0.001	495382	710	30320	$4f^{13}5p^6$	$^2F_{5/2}$	17410	$4f^{13}5p^55d$	7/2	512790
202.250	0.000	494437	330	1336	$4f^{14}5p^5$	$^2P_{1/2}$	89123	$4f^{14}5p^46s$	3/2	583560
203.623	0.000	491104	310	8110	$4f^{14}5p^5$	$^2P_{3/2}$	1233	$4f^{14}5p^45d$	1/2	492337
205.221	0.001	487280	620	6384	$4f^{13}5p^6$	$^2F_{5/2}$	17410	$4f^{12}5p^65d$	3/2	504691
205.479		486668	660	3063	$4f^{14}5p^5$	$^2P_{3/2}$	1233	$4f^{14}5p^46s$	3/2	487901
206.634	−0.002	483947	340	1646	$4f^{14}5p^5$	$^2P_{3/2}$	1233	$4f^{13}5p^55d$	5/2	485175
207.092	0.002	482878	270	746	$4f^{14}5p^5$	$^2P_{1/2}$	89123	$4f^{14}5p^46s$	1/2	572004
207.466	0.001	482007	340	2816	$4f^{14}5p^5$	$^2P_{3/2}$	1233	$4f^{13}5p^55d$	3/2	483243
207.690	−0.006	481488	43	137	$4f^{13}5p^6$	$^2F_{7/2}$	0	$4f^{14}5p^46s$	5/2	481473
207.736	0.001	481381	170	252	$4f^{13}5p^6$	$^2F_{5/2}$	17410	$4f^{13}5p^55d$	7/2	498792
207.850	0.007	481116	51	54	$4f^{13}5p^6$	$^2F_{5/2}$	17410	$4f^{14}5p^45d$	3/2	498541
207.884	−0.001	481038	260	813	$4f^{13}5p^6$	$^2F_{7/2}$	0	$4f^{14}5p^45d$	5/2	481035
208.227	−0.002	480245	170	176	$4f^{14}5p^5$	$^2P_{3/2}$	1233	$4f^{14}5p^46s$	5/2	481473
208.420	0.001	479800	660	14526	$4f^{14}5p^5$	$^2P_{3/2}$	1233	$4f^{14}5p^45d$	5/2	481035
208.543	0.002	479517	490	5119	$4f^{14}5p^5$	$^2P_{1/2}$	89123	$4f^{14}5p^46s$	3/2	568644
209.175	0.000	478070	370	6942	$4f^{14}5p^5$	$^2P_{1/2}$	89123	$4f^{14}5p^46s$	3/2	567191
211.027	0.005	473873	670	4427	$4f^{14}5p^5$	$^2P_{3/2}$	1233	$4f^{14}5p^45d$	3/2	475117
213.436	−0.001	468524	130	3	$4f^{13}5p^6$	$^2F_{7/2}$	0	$4f^{12}5p^65d$	5/2	468523
213.661	0.001	468030	42	2	$4f^{13}5p^6$	$^2F_{7/2}$	0	$4f^{12}5p^65d$	5/2	468034
213.785	0.003	467759	27	130	$4f^{13}5p^6$	$^2F_{5/2}$	17410	$4f^{13}5p^55d$	5/2	485175
214.001	0.001	467287	170	140	$4f^{14}5p^5$	$^2P_{3/2}$	1233	$4f^{12}5p^65d$	5/2	468523
214.229	0.005	466791	690	2080	$4f^{14}5p^5$	$^2P_{3/2}$	1233	$4f^{12}5p^65d$	5/2	468034
214.488	−0.003	466226	15	7	$4f^{13}5p^6$	$^2F_{7/2}$	0	$4f^{12}5p^65d$	5/2	466219
215.055	−0.005	464996	600	946	$4f^{14}5p^5$	$^2P_{3/2}$	1233	$4f^{12}5p^65d$	5/2	466219
215.496	0.008	464046	26	7	$4f^{13}5p^6$	$^2F_{5/2}$	17410	$4f^{14}5p^46s$	5/2	481473
215.692	0.001	463624	69	83	$4f^{13}5p^6$	$^2F_{5/2}$	17410	$4f^{14}5p^45d$	5/2	481035
216.596	0.002	461689	460	369	$4f^{14}5p^5$	$^2P_{3/2}$	1233	$4f^{12}5p^65d$	3/2	462927
217.601	0.006	459556	64	16	$4f^{13}5p^6$	$^2F_{7/2}$	0	$4f^{12}5p^65d$	5/2	459570
218.174	−0.006	458350	350	28	$4f^{14}5p^5$	$^2P_{3/2}$	1233	$4f^{12}5p^65d$	5/2	459570

Table 1. *Cont.*

λ (Å)[h]	o-c[a] (Å)	σ (cm^{-1})	Int.	gA ($10^8 \cdot s^{-1}$)	Lower Level			Upper Level		
					Config.[b]	Term	E (cm^{-1})	Config.[c]	J	E(cm^{-1})
218.429		457814	550	215	$4f^{13}5p^6$	$^2F_{7/2}$	0	$4f^{12}5p^65d$	9/2	457815
218.477	−0.003	457714	33	17	$4f^{13}5p^6$	$^2F_{5/2}$	17410	$4f^{14}5p^45d$	3/2	475117
218.507	0.000	457651	400	118	$4f^{13}5p^6$	$^2F_{7/2}$	0	$4f^{13}5p^55d$	5/2	457652
218.747	−0.001	457148	180	238	$4f^{14}5p^5$	$^2P_{3/2}$	1233	$4f^{12}5p^65d$	3/2	458380
219.097	0.000	456419	20	1	$4f^{14}5p^5$	$^2P_{3/2}$	1233	$4f^{13}5p^55d$	5/2	457652
220.239	0.007	454053	16	2	$4f^{13}5p^6$	$^2F_{7/2}$	0	$4f^{12}5p^65d$	7/2	454067
221.443	0.002	451583	600	483	$4f^{14}5p^5$	$^2P_{3/2}$	1233	$4f^{12}5p^65d$	3/2	452821
221.908	−0.006	450637	220	260	$4f^{13}5p^6$	$^2F_{5/2}$	17410	$4f^{12}5p^65d$	5/2	468034
222.818	0.006	448797	33	65	$4f^{13}5p^6$	$^2F_{5/2}$	17410	$4f^{12}5p^65d$	5/2	466219
223.260	0.000	447908	62	67	$4f^{13}5p^6$	$^2F_{7/2}$	0	$4f^{12}5p^65d$	5/2	447909
224.573	−0.002	445289	9	6	$4f^{13}5p^6$	$^2F_{7/2}$	0	$4f^{12}5p^65d$	5/2	445286
225.203	0.005	444044	110	39	$4f^{14}5p^5$	$^2P_{3/2}$	1233	$4f^{12}5p^65d$	5/2	445286
227.497	−0.003	439566	340	200	$4f^{13}5p^6$	$^2F_{7/2}$	0	$4f^{12}5p^65d$	7/2	439561
227.519	0.003	439523	56	13	$4f^{14}5p^5$	$^2P_{1/2}$	89123	$4f^{13}5p^56s$	3/2	528652
227.617	0.003	439335	440	5786	$4f^{14}5p^5$	$^2P_{1/2}$	89123	$4f^{14}5p^45d$	1/2	528462
229.011	−0.002	436661	410	186	$4f^{13}5p^6$	$^2F_{5/2}$	17410	$4f^{12}5p^65d$	7/2	454067
229.541	0.003	435652	490	15	$4f^{13}5p^6$	$^2F_{7/2}$	0	$4f^{14}5p^45d$	7/2	435658
229.590	0.001	435558	160	125	$4f^{13}5p^6$	$^2F_{7/2}$	0	$4f^{12}5p^65d$	5/2	435561
229.666	−0.002	435415	58	29	$4f^{13}5p^6$	$^2F_{5/2}$	17410	$4f^{12}5p^65d$	3/2	452821
230.246	0.005	434318	210	156	$4f^{14}5p^5$	$^2P_{3/2}$	1233	$4f^{12}5p^65d$	5/2	435561
230.544	0.001	433757	5	603	$4f^{14}5p^5$	$^2P_{1/2}$	89123	$4f^{12}5p^65d$	3/2	522881
230.964	−0.003	432967	75	57	$4f^{13}5p^6$	$^2F_{7/2}$	0	$4f^{12}5p^65d$	5/2	432963
231.629	0.003	431725	510	319	$4f^{14}5p^5$	$^2P_{3/2}$	1233	$4f^{12}5p^65d$	5/2	432963
232.176		430708	460	109	$4f^{13}5p^6$	$^2F_{7/2}$	0	$4f^{12}5p^65d$	7/2	430708
232.288	0.000	430499	440	195	$4f^{13}5p^6$	$^2F_{5/2}$	17410	$4f^{12}5p^65d$	5/2	447909
233.225	0.004	428771	840	425	$4f^{13}5p^6$	$^2F_{7/2}$	0	$4f^{12}5p^65d$	7/2	428777
233.525	−0.002	428221	190	196	$4f^{13}5p^6$	$^2F_{7/2}$	0	$4f^{12}5p^65d$	7/2	428216
233.709	−0.003	427883	550	328	$4f^{13}5p^6$	$^2F_{5/2}$	17410	$4f^{12}5p^65d$	5/2	445286
235.418	0.003	424776	140	78	$4f^{13}5p^6$	$^2F_{7/2}$	0	$4f^{12}5p^65d$	5/2	424781
235.509	−0.001	424612	47	10	$4f^{14}5p^5$	$^2P_{3/2}$	1233	$4f^{12}5p^65d$	3/2	425843
236.884	0.002	422148	29	117	$4f^{13}5p^6$	$^2F_{5/2}$	17410	$4f^{12}5p^65d$	7/2	439561
238.243		419739	310	125	$4f^{13}5p^6$	$^2F_{5/2}$	17410	$4f^{12}5p^65d$	5/2	437149
238.330	−0.001	419586	24	6	$4f^{13}5p^6$	$^2F_{7/2}$	0	$4f^{12}5p^65d$	7/2	419585
239.004		418402	280	119	$4f^{13}5p^6$	$^2F_{7/2}$	0	$4f^{12}5p^65d$	9/2	418403
239.089	−0.003	418255	580	2	$4f^{13}5p^6$	$^2F_{5/2}$	17410	$4f^{14}5p^45d$	7/2	435658
239.142	−0.006	418162	150	101	$4f^{13}5p^6$	$^2F_{5/2}$	17410	$4f^{12}5p^65d$	5/2	435561
240.107		416480	810	499	$4f^{13}5p^6$	$^2F_{7/2}$	0	$4f^{12}5p^65d$	9/2	416481
240.468	−0.002	415855	10	9	$4f^{13}5p^6$	$^2F_{7/2}$	0	$4f^{12}5p^65d$	5/2	415852
240.634	0.000	415569	26	728	$4f^{14}5p^5$	$^2P_{1/2}$	89123	$4f^{12}5p^65d$	3/2	504691
241.037	0.008	414874	69	89	$4f^{13}5p^6$	$^2F_{7/2}$	0	$4f^{12}5p^65d$	7/2	414888
241.183	−0.002	414623	12	7	$4f^{14}5p^5$	$^2P_{3/2}$	1233	$4f^{12}5p^65d$	5/2	415852
241.867		413451	960	716	$4f^{13}5p^6$	$^2F_{7/2}$	0	$4f^{12}5p^65d$	9/2	413450
242.819	0.002	411829	420	72	$4f^{13}5p^6$	$^2F_{7/2}$	0	$4f^{12}5p^65d$	7/2	411832

Table 1. *Cont.*

λ (Å)[h]	o-c[a] (Å)	σ (cm^{-1})	Int.	gA ($10^8 \cdot s^{-1}$)	Lower Level			Upper Level		
					Config.[b]	Term	E (cm^{-1})	Config.[c]	J	E(cm^{-1})
242.829	0.004	411813	270	17	$4f^{13}5p^6$	$^2F_{7/2}$	0	$4f^{12}5p^65d$	5/2	411819
243.088	−0.004	411374	52	26	$4f^{13}5p^6$	$^2F_{5/2}$	17410	$4f^{12}5p^65d$	7/2	428777
243.426	0.002	410802	120	21	$4f^{13}5p^6$	$^2F_{5/2}$	17410	$4f^{12}5p^65d$	7/2	428216
243.434		410788	260	36	$4f^{13}5p^6$	$^2F_{5/2}$	17410	$4f^{12}5p^65d$	3/2	428199
243.518	0.004	410647	10	10	$4f^{13}5p^6$	$^2F_{7/2}$	0	$4f^{12}5p^65d$	7/2	410654
243.551	−0.003	410591	7	17	$4f^{14}5p^5$	$^2P_{3/2}$	1233	$4f^{12}5p^65d$	5/2	411819
244.281	−0.002	409364	330	74	$4f^{13}5p^6$	$^2F_{7/2}$	0	$4f^{12}5p^65d$	5/2	409362
244.833	0.001	408442	190	52	$4f^{14}5p^5$	$^2P_{3/2}$	1233	$4f^{12}5p^65d$	5/2	409676
244.839	0.001	408431	150	102	$4f^{13}5p^6$	$^2F_{5/2}$	17410	$4f^{12}5p^65d$	3/2	425843
245.046	0.000	408087	580	191	$4f^{13}5p^6$	$^2F_{7/2}$	0	$4f^{12}5p^65d$	7/2	408086
245.334	−0.005	407607	12	14	$4f^{14}5p^5$	$^2P_{3/2}$	1233	$4f^{12}5p^65d$	3/2	408833
245.474	−0.002	407375	470	74	$4f^{13}5p^6$	$^2F_{5/2}$	17410	$4f^{12}5p^65d$	5/2	424781
246.362		405907	780	291	$4f^{13}5p^6$	$^2F_{7/2}$	0	$4f^{12}5p^65d$	9/2	405907
248.007	0.000	403215	36	104	$4f^{14}5p^5$	$^2P_{1/2}$	89123	$4f^{14}5p^45d$	1/2	492337
248.508		402401	490	262	$4f^{13}5p^6$	$^2F_{5/2}$	17410	$4f^{12}5p^65d$	5/2	419811
248.649	0.001	402174	690	329	$4f^{13}5p^6$	$^2F_{5/2}$	17410	$4f^{12}5p^65d$	7/2	419585
248.765	−0.001	401985	810	676	$4f^{13}5p^6$	$^2F_{7/2}$	0	$4f^{14}5p^45d$	5/2	401984
249.533	0.001	400748	960	1369	$4f^{14}5p^5$	$^2P_{3/2}$	1233	$4f^{14}5p^45d$	5/2	401984
249.873		400203	820	340	$4f^{13}5p^6$	$^2F_{7/2}$	0	$4f^{12}5p^65d$	9/2	400203
250.010		399984	190	104	$4f^{13}5p^6$	$^2F_{5/2}$	17410	$4f^{12}5p^65d$	3/2	417394
250.811		398706	120	106	$4f^{13}5p^6$	$^2F_{7/2}$	0	$4f^{13}5p^55d$	9/2	398707
250.978	0.001	398441	420	126	$4f^{13}5p^6$	$^2F_{5/2}$	17410	$4f^{12}5p^65d$	5/2	415852
251.500	−0.001	397614	340	87	$4f^{13}5p^6$	$^2F_{7/2}$	0	$4f^{12}5p^65d$	5/2	397612
251.584	−0.002	397481	790	528	$4f^{13}5p^6$	$^2F_{5/2}$	17410	$4f^{12}5p^65d$	7/2	414888
252.203	−0.001	396506	960	591	$4f^{13}5p^6$	$^2F_{7/2}$	0	$4f^{13}5p^55d$	7/2	396505
252.285	0.001	396377	320	109	$4f^{14}5p^5$	$^2P_{3/2}$	1233	$4f^{12}5p^65d$	5/2	397612
252.740	−0.002	395664	930	1471	$4f^{14}5p^5$	$^2P_{3/2}$	1233	$4f^{13}5p^55d$	3/2	396894
252.862	−0.001	395473	790	2	$4f^{13}5p^6$	$^2F_{7/2}$	0	$4f^{13}5p^55d$	7/2	395471
252.989	0.001	395274	210	48	$4f^{13}5p^6$	$^2F_{7/2}$	0	$4f^{13}5p^55d$	5/2	395276
253.534	−0.001	394424	590	187	$4f^{13}5p^6$	$^2F_{5/2}$	17410	$4f^{12}5p^65d$	7/2	411832
253.541	−0.003	394413	820	1411	$4f^{13}5p^6$	$^2F_{5/2}$	17410	$4f^{12}5p^65d$	5/2	411819
253.653	0.001	394239	710	443	$4f^{14}5p^5$	$^2P_{3/2}$	1233	$4f^{14}5p^45d$	1/2	395474
253.726	−0.004	394126	23	14	$4f^{14}5p^5$	$^2P_{1/2}$	89123	$4f^{13}5p^55d$	3/2	483243
253.779	−0.001	394043	71	7	$4f^{14}5p^5$	$^2P_{3/2}$	1233	$4f^{13}5p^55d$	5/2	395276
253.812		393992	1000	1960	$4f^{13}5p^6$	$^2F_{7/2}$	0	$4f^{12}5p^65d$	7/2	393992
254.294	−0.001	393245	930	1535	$4f^{13}5p^6$	$^2F_{5/2}$	17410	$4f^{12}5p^65d$	7/2	410654
254.551		392849	1000	1392	$4f^{13}5p^6$	$^2F_{5/2}$	17410	$4f^{12}5p^65d$	3/2	410258
254.928	−0.001	392267	440	168	$4f^{13}5p^6$	$^2F_{5/2}$	17410	$4f^{12}5p^65d$	5/2	409676
255.140	0.007	391942	6	34	$4f^{13}5p^6$	$^2F_{5/2}$	17410	$4f^{12}5p^65d$	5/2	409362
255.401		391541	860	2981	$4f^{13}5p^6$	$^2F_{7/2}$	0	$4f^{13}5p^55d$	9/2	391541
255.479	0.001	391422	200	110	$4f^{13}5p^6$	$^2F_{5/2}$	17410	$4f^{12}5p^65d$	3/2	408833
255.967	0.001	390675	390	510	$4f^{13}5p^6$	$^2F_{5/2}$	17410	$4f^{12}5p^65d$	7/2	408086
258.592	−0.004	386710	980	1433	$4f^{13}5p^6$	$^2F_{7/2}$	0	$4f^{13}5p^55d$	5/2	386704
259.069	−0.002	385998	280	154	$4f^{14}5p^5$	$^2P_{1/2}$	89123	$4f^{14}5p^45d$	3/2	475117
259.419	−0.004	385476	920	633	$4f^{14}5p^5$	$^2P_{3/2}$	1233	$4f^{13}5p^55d$	5/2	386704

Table 1. *Cont.*

λ (Å)[h]	o-c[a] (Å)	σ (cm^{-1})	Int.	gA ($10^8 \cdot s^{-1}$)	Lower Level			Upper Level		
					Config.[b]	Term	E (cm^{-1})	Config.[c]	J	E(cm^{-1})
260.027	−0.001	384576	14	31	$4f^{13}5p^6$	$^2F_{5/2}$	17410	$4f^{14}5p^45d$	5/2	401984
260.146		384400	290	54	$4f^{13}5p^6$	$^2F_{7/2}$	0	$4f^{13}5p^55d$	9/2	384400
261.002	−0.004	383139	5	49	$4f^{13}5p^6$	$^2F_{7/2}$	0	$4f^{13}5p^55d$	5/2	383133
261.767		382019	680	155	$4f^{13}5p^6$	$^2F_{7/2}$	0	$4f^{13}5p^55d$	7/2	382019
261.849	0.000	381899	450	15	$4f^{14}5p^5$	$^2P_{3/2}$	1233	$4f^{13}5p^55d$	5/2	383133
262.537		380899	530	53	$4f^{13}5p^6$	$^2F_{7/2}$	0	$4f^{13}5p^55d$	9/2	380899
263.521	0.006	379476	23	1	$4f^{13}5p^6$	$^2F_{5/2}$	17410	$4f^{13}5p^55d$	3/2	396894
263.787	0.001	379094	300	73	$4f^{13}5p^6$	$^2F_{5/2}$	17410	$4f^{13}5p^55d$	7/2	396505
264.508	0.001	378060	23	85	$4f^{13}5p^6$	$^2F_{5/2}$	17410	$4f^{13}5p^55d$	7/2	395471
264.644[d]	0.001	377867	320	111	$4f^{13}5p^6$	$^2F_{7/2}$	0	$4f^{13}5p^55d$	5/2	377867
264.644[d]	0.000	377867	320	72	$4f^{13}5p^6$	$^2F_{5/2}$	17410	$4f^{13}5p^55d$	5/2	395276
265.168		377120	460	133	$4f^{13}5p^6$	$^2F_{7/2}$	0	$4f^{13}5p^55d$	9/2	377119
265.510	0.000	376633	30	78	$4f^{14}5p^5$	$^2P_{3/2}$	1233	$4f^{13}5p^55d$	5/2	377867
265.919	0.000	376054	400	11	$4f^{14}5p^5$	$^2P_{3/2}$	1233	$4f^{13}5p^55d$	3/2	377288
267.518	−0.002	373807	74	3	$4f^{14}5p^5$	$^2P_{1/2}$	89123	$4f^{12}5p^65d$	3/2	462927
270.794	0.007	369284	51	2	$4f^{13}5p^6$	$^2F_{5/2}$	17410	$4f^{13}5p^55d$	5/2	386704
270.816	0.002	369254	10	76	$4f^{14}5p^5$	$^2P_{1/2}$	89123	$4f^{12}5p^65d$	3/2	458380

[a] The difference between the observed wavelength and the wavelength derived from the final level energies (Ritz wavelength). A blank value indicates that the upper level is derived from that line only; [b] The closed subshell $5s^2$ is omitted from configuration labelling; [c] Configuration attribution is arbitrary in a few cases (see text); [d] Doubly identified; [e] Questionable identification; [h] Estimated uncertainty ±0.005 Å.

Lu V The unique analysis of Lu V by Kaufman and Sugar [20] reports transitions between the configurations $4f^{13}$, $4f^{12}5d$, $4f^{12}6s$, and $4f^{12}6p$. In addition to levels with the highest J-values often established from one single strong line, several levels were derived from two transitions according to selection rules taking into account the J-J coupling scheme that dominates in the $4f^{12}6s$ and $4f^{12}6p$ configurations, and the intermediate coupling between LS and J-J limits in the $4f^{12}5d$ configuration. However, no transition probabilities were reported. Indeed, large hyperfine structures could not be resolved because of the line broadening in the high-current spark used, and consequently their line list contained many blends and 15 doubly classified lines [20].

In the present work, parametric calculations were performed with the Cowan codes and the agreement between the intensities of classified lines and the calculated transition probabilities was checked. We paid attention to several unknown levels, mostly with small J-values and relatively weak transition probabilities. In the absence of new observations of lutetium spark spectra, the unique set of data available for extending the Lu V analysis is an unpublished line list of wavelengths initially considered as Lu V by Kaufman and Sugar before 1980 [21]. As transitions between high levels of Lu IV were excited under conditions similar to Lu V, some of these lines [21] were later interpreted as the $4f^{13}5f$–$4f^{13}5d$ transitions of Lu IV in [22], the corresponding transition array being traced up from Lu IV to W VII. As for Lu V, by comparing the transition probabilities for missing levels to the intensities of assumed Lu V lines, the following levels have been determined from some of their most probable transitions:

E = 291733.0 ($4f^{12}$ $^3P_2$, $6p_{1/2}$) J = 3/2,
E = 291764.8 ($4f^{12}$ $^3P_2$, $6p_{1/2}$) J = 5/2,
E = 296226.7 ($4f^{12}$ $^1G_4$, $6p_{3/2}$) J = 5/2,
E = 160846.4 ($4f^{12}$ $^3H_4$, $5d_{5/2}$) J = 3/2,
E = 176831.6 ($4f^{12}$ $^3F_3$, $5d_{5/2}$) J = 11/2,
E = 177390.0 ($4f^{12}$ $^3F_3$, $5d_{5/2}$) J = 5/2,
E = 197304.0 ($4f^{12}$ $^1I_6$, $5d_{3/2}$) J = 13/2.

Table 2 gives 20 lines used for the present determination of new levels. Three of them are doubly identified. Two of these, 563.723 Å and 880.543 Å, were already reported in [20] with different identifications. All the other lines are from the line list of [21]. One weak line has been identified as the transition between previously known levels [20] confirming the latter. The absence of a predicted strong transition 313347.6 ($4f^{12}$ $^1I_6$, $6p_{3/2}$) 9/2–243552.86 ($4f^{12}$ $^1I_6$, $6s_{1/2}$) 11/2 with gA = 1.456 × 10^{10} s^{-1} and Ritz wavelength 1495.488 Å in the available line lists is unexplained. In the case of the isoelectronic spectrum Yb IV, a similar situation had been the starting point of a revised analysis [23].

Table 2. Newly identified lines of Lu V. Experimental wavelengths (estimated uncertainty ±0.005 Å) and intensities (in arbitrary units) are taken from the line list of [21]. Calculated gA values are from the present work.

λ_{exp} (Å)	λ_{Ritz} (Å)	σ_{Ritz} (cm^{-1})	Intensity (arb.)	gA ($10^6 \cdot s^{-1}$)	E_{odd} (cm^{-1})	J_{odd}	E_{even} (cm^{-1})	J_{even}
563.723 [a,d]	563.708	177396.9	100	425	0.0	7/2	177396.9	9/2
563.723 [a,d]	563.730	177390.0	100	2108	0.0	7/2	177390.0	5/2
786.582	786.572	127134.0	1	67	287980.4	5/2	160846.4	3/2
806.043	806.046	124062.4	1	668	284908.8	5/2	160846.4	3/2
856.592	856.593	116741.5	6	1552	277587.9	5/2	160846.4	3/2
874.638	874.640	114332.7	6	2451	296226.7	5/2	181894.0	7/2
875.645	875.644	114201.7	6	3034	296226.7	5/2	182025.0	5/2
880.543 [b,d]	880.534	113567.5	20	3306	274413.9	5/2	160846.4	3/2
880.543 [b,d]	880.556	113564.6	20	4832	280099.9	7/2	166535.3	7/2
898.980	898.985	111236.6	40	15750	288068.2	9/2	176831.6	11/2
909.941	909.941	109897.2	1	797	287287.2	5/2	177390.0	5/2
910.156	910.160	109870.8	4	1693	291764.8	5/2	181894.0	7/2
911.242	911.246	109739.8	5	2090	291764.8	5/2	182025.0	5/2
911.509	911.511	109708.0	5	1915	291733.0	3/2	182025.0	5/2
914.012	914.012	109407.8	3	1327	296226.7	5/2	186818.9	5/2
914.326	914.326	109370.2	3	910	286201.8	9/2	176831.6	11/2
919.071	919.076	108804.9	3	654	286201.8	9/2	177396.9	9/2
920.269	920.265	108664.3	3	901	285495.9	11/2	176831.6	11/2
952.873	952.872	104945.9	1	1638	291764.8	5/2	186818.9	5/2
953.165	953.161	104914.1	1	1317	291733.0	3/2	186818.9	5/2
974.890 [d]	974.886	102576.1	1	1498	291764.8	5/2	189188.7	7/2
974.890 [d]	974.889	102575.8	1	5339	299879.8	11/2	197304.0	13/2
978.015	978.017	102247.7	4	9081	299551.7	13/2	197304.0	13/2

[a] Line already reported in [20] now interpreted as a blend of two resonance transitions with different gA values; [b] Line already reported in [20] now interpreted as a blend of two transitions with close gA values; [d] Doubly identified.

Hf VI [11]. A total of 189 lines in the region 193–474 Å were identified in our spectra. In comparison with W VIII, the analysis was extended by the identification of the $4f^{13}5s^25p^6$–$4f^{12}5s^25p^66d$ transitions. The interaction between the $4f^{13}5s^25p^55d$ and the $4f^{12}5s^25p^66s$ configurations appeared to be very important in this spectrum. The $4f^{12}5s^25p^66s$ levels were not established, but this configuration is present as the second or the third component of several $4f^{13}5s^25p^55d$ levels that helped to estimate its average energy by the appropriate fitting of calculations to measured level energies. Fine structure splittings and relative positions of the odd terms were established, and 142 levels of the excited, even configurations were found.

Ta VII [12]. The same set of transitions as in W VIII was studied in Ta VII in our observed spectra. A total of 237 lines in the region 191–354 Å were identified as transitions between four odd, low-lying levels and 126 even, excited levels. The $4f^{12}5s^25p^66s$ configuration in Ta VII, contrary to Hf VI, only partly overlaps with the upper part of the $4f^{12}5s^25p^65d$ configuration, and does not undergo a strong interaction from the latter. On the other hand, the $4f^{12}5s^25p^66s$ configuration strongly interacts with the $4f^{13}5s^25p^56s$, $4f^{14}5s^25p^46s$, and $4f^{14}5s^25p^45d$ configurations. The levels of the $4f^{12}5s^25p^66s$ configuration have large contributions from these three configurations, resulting in the observation of many "forbidden" E1 transitions to both low-lying $4f^{13}5s^25p^6$ and $4f^{14}5s^25p^5$ configurations. Six energy levels of the $4f^{12}5s^25p^66s$ configuration were found, which permitted the $4f^{12}5s^25p^66s$ configuration to be explicitly included in the parametric description of the Ta VII even energy levels.

Re IX [13]. Unlike the previous isoelectronic spectra Hf VI–W VIII, where the ground level is $4f^{13}5s^25p^6\ ^2F_{7/2}$, Re IX is the first spectrum in the isoelectronic sequence where the ground level is found to be $4f^{14}5s^25p^5\ ^2P_{3/2}$, whereas the $4f^{13}5s^25p^6\ ^2F_{7/2}$ level is located 63,439 cm^{-1} above it. The $4f^{12}5s^25p^66s$ configuration now lies above all the other even configurations that give the resonance transitions, and their mutual interactions are not as important as in the previous spectra. A total of 112 lines in the region 146–244 Å have been identified in our observed spectra and 87 levels have been found.

As was mentioned in Section 2, the spectra (energy levels, wavelengths, and transition probabilities) were calculated with the use of Cowan codes [18]. In these calculations, *ab initio* Hartree-Fock values of radial integrals are improved by fitting the theoretical to experimental energy levels. In a case as complex as these spectra, involving strong interaction between seven configurations based on open 4f, 5s, and 5p sub-shells, the fitting process meets divergence problems if too many parameters are left free. Table 3, where the fitted energy parameters (FIT) for W VIII are listed, shows the numerous constraints applied. Due to this situation, the standard deviations of the fits, 340, 380, 440, and 494 cm^{-1} in Hf VI, Ta VII, W VIII and Re IX, respectively, are larger than in lower Z elements of the same sequence in which configuration interactions are weaker. For instance, a standard deviation of 77 cm^{-1} was obtained for the even configurations $4f^{12}(5d+6s+6d+7s)$ in Yb IV [23] and 54 cm^{-1} for the even configurations $4f^{12}(5d+6s)$ in Lu V [20].

Table 3. Fitted (FIT) energy parameters (in cm^{-1}) of W VIII with uncertainties of their definition (Unc.) in comparison with the HFR parameters.

Configuration	Parameter	FIT	Unc.	Status [a]	HFR	FIT/HFR [b]
Odd						
$4f^{13}5s^25p^6$	E_{av}	7461	0		7546	−85
	ζ(4f)	4974	0		5030	0.989
$4f^{14}5s^25p^5$	E_{av}	30529	0		40520	−9991
	ζ(5p)	58593	0		58976	0.994
Even						
$4f^{14}5s5p^6$	E_{av}	377512		f	384795	−7283
$4f^{13}5s^25p^55d$	E_{av}	403014	241		399311	3703
	ζ(4f)	5020	42	r11	5045	0.995
	ζ(5p)	60627	116	r2	61713	0.982
	ζ(5d)	4668	109	r10	4773	0.978
	F^2(4f,5p)	52499	1446	r12	67376	0.779
	F^2(4f,5d)	33847	1845	r4	45326	0.747
	F^4(4f,5d)	16437	896	r4	22012	0.747
	F^2(5p,5d)	65257	2675	r7	78482	0.831
	G^2(4f,5p)	28419	1152	r3	27466	1.035
	G^4(4f,5p)	23650	959	r3	22857	1.035
	G^1(4f,5d)	14185	369	r5	15975	0.888
	G^3(4f,5d)	13292	346	r5	14969	0.888
	G^5(4f,5d)	10627	277	r5	11968	0.888
	G^1(5p,5d)	67784	615	r1	95279	0.711
	G^3(5p,5d)	42727	388	r1	60060	0.711
$4f^{13}5s^25p^56d$	E_{av}	775400		f	772171	3229
$4f^{13}5s^25p^56s$	E_{av}	542202	127		541049	1153
	ζ(4f)	5031	42	r11	5059	0.994
	ζ(5p)	61816	118	r2	62925	0.982
	F^2(4f,5p)	53015	1460	r12	68041	0.779
	G^2(4f,5p)	28612	1160	r3	27671	1.034
	G^4(4f,5p)	23881	968	r3	23081	1.035
	G^3(4f,6s)	6291	1804		5312	1.184
	G^1(5p,6s)	9567	686	r13	10655	0.898
$4f^{13}5s^25p^57s$	E_{av}	813134		f	813134	0
$4f^{14}5s^25p^45d$	E_{av}	420075	415		426261	−6186
	F^2(5p,5p)	76605	2809	r14	92368	0.829
	ζ(5p)	58700	112	r2	59661	0.984
	ζ(5d)	4419	104	r10	4520	0.978
	F^2(5p,5d)	64116	2628	r7	77107	0.832
	G^1(5p,5d)	66465	603	r1	93327	0.712
	G^3(5p,5d)	41891	380	r1	58821	0.712
$4f^{14}5s^25p^46d$	E_{av}	778313		f	786313	−8000
$4f^{14}5s^25p^46s$	E_{av}	550168	240		557405	−7237
	F^2(5p,5p)	77497	2842	r14	92990	0.833
	ζ(5p)	59855	114	r2	60835	0.984
	G^1(5p,6s)	9579	687	r13	10669	0.898
$4f^{14}5s^25p^47s$	E_{av}	813793		f	825793	−12000
$4f^{14}5s5p^56p$	E_{av}	992590		f	992590	0
$4f^{14}5s5p^55f$	E_{av}	1092223		f	1092223	0

Table 3. *Cont.*

Configuration	Parameter	FIT	Unc.	Status [a]	HFR	FIT/HFR [b]
$4f^{12}5s^25p^65d$	E_{av}	429242	123		417114	12128
	$F^2(4f,4f)$	148220	2174		176787	0.838
	$F^4(4f,4f)$	106797	6059		112472	0.95
	$F^6(4f,4f)$	72685	3157		81373	0.893
	α(4f)	22		f	0	
	β(4f)	−1000		f	0	
	γ(4f)	−70		f	0	
	ζ(4f)	5198	43	r11	5227	0.994
	ζ(5d)	4926	115	r10	5038	0.978
	$F^2(4f,5d)$	36271	1297	r6	46227	0.785
	$F^4(4f,5d)$	17578	629	r6	22404	0.785
	$G^1(4f,5d)$	14023	365	r5	15792	0.888
	$G^3(4f,5d)$	13329	347	r5	15011	0.888
	$G^5(4f,5d)$	10710	279	r5	12062	0.888
$4f^{12}5s^25p^66d$	E_{av}	819431		f	803431	16000
$4f^{12}5s^25p^66s$	E_{av}	579803		f	570086	9717
	$F^2(4f,4f)$	147636		f	177235	0.833
	$F^4(4f,4f)$	110752		f	112783	0.982
	$F^6(4f,4f)$	78585		f	81606	0.963
	α(4f)	22		f	0	
	β(4f)	−1000		f	0	
	γ(4f)	−70		f	0	
	ζ(4f)	5161		f	5241	0.985
	$G^3(4f,6s)$	3974		f	5245	0.758
$4f^{13}5s^25p^55d$–$5s^25p^45d$	$D^2(4f,5p,4f,4f)$	−5660	99	r8	−6553	0.864
	$D^4(4f,5p,4f,4f)$	−309	5	r8	−359	0.864
	$D^2(5p,5p,4f,5p)$	−34863	611	r8	−40359	0.864
	$D^2(5p,5d,4f,5d)$	−27245	478	r8	−31540	0.864
	$D^4(5p,5d,4f,5d)$	−17854	313	r8	−20669	0.864
	$E^1(5p,5d,4f,5d)$	−24106	423	r8	−27907	0.864
	$E^3(5p,5d,4f,5d)$	−18066	317	r8	−20915	0.864
$4f^{13}5s^25p^55d$–$4f^{12}5s^25p^65d$	$D^2(4f,4f,4f,5p)$	−3787	52	r9	−4586	0.826
	$D^4(4f,4f,4f,5p)$	857	12	r9	1039	0.826
	$D^2(4f,5p,5p,5p)$	−32514	444	r9	−39373	0.826
	$D^2(4f,5d,5p,5d)$	−25571	349	r9	−30966	0.826
	$D^4(4f,5d,5p,5d)$	−16823	230	r9	−20372	0.826
	$E^1(4f,5d,5p,5d)$	−22364	305	r9	−27081	0.826
	$E^3(4f,5d,5p,5d)$	−16960	231	r9	−20538	0.826
$4f^{14}5s^25p^45d$–$4f^{12}5s^25p^65d$	$D^2(4f,4f,5p,5p)$	24561	335	r9	29743	0.826
	$D^4(4f,4f,5p,5p)$	20265	277	r9	24540	0.826
$4f^{13}5s^25p^56s$–$4f^{14}5s^25p^46s$	$D^2(4f,5p,4f,4f)$	−6391		f		1.0
	$D^4(4f,5p,4f,4f)$	−244		f		1.0
	$D^2(5p,5p,4f,5p)$	−40487		f		1.0

[a] f—fixed parameter, rn, n = 1–14—parameters linked by their corresponding HFR ratios; [b] For E_{av}, the difference between the fitted and *ab initio* values is given; the omitted electrostatic parameters of unknown configurations, as well as interaction parameters not listed in the table, are scaled by a factor of 0.85 with respect to the *ab initio* values; the omitted spin-orbit parameters are not scaled.

The spectra are calculated with the use of the fitted energy parameters. Table 3 also contains so-called scaling factors: ratios of the fitted to Hartree-Fock parameters (FIT/HFR). It is important that the scaling factors behave regularly along the isoelectronic sequence. For the average energies of configurations, instead of the scaling factors, the differences between fitted and *ab initio* values are shown in Figure 4. To guide the eye, straight lines connect the points in Figure 4. The points related to the $4f^{12}5s^25p^66s$ configuration (brown squares) are not connected because fittings were performed only in Lu V [20] and Ta VII [12] and the corresponding points are only roughly estimated in Hf VI [11] and W VIII [10]. It is seen that the differences between fitted and Hartree-Fock average energies of configurations are similar for groups of the same 4f sub-shell and progress quite regularly along the isoelectronic sequence.

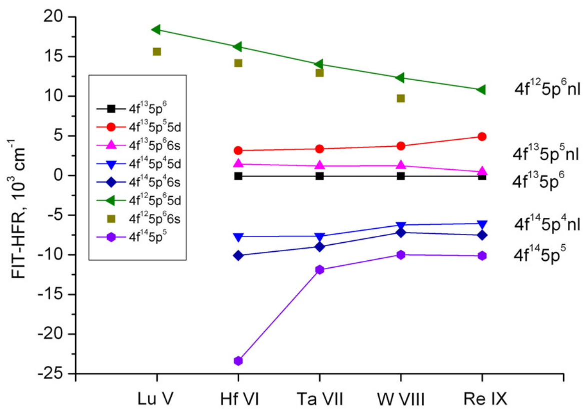

Figure 4. Differences between the experimental and HFR average energies of configurations in the W VIII isoelectronic sequence.

The scaling factors for electrostatic energy parameters are presented in Figures 5 and 6. They represent all electrostatic energy parameters in the configurations with the $4f^{14}$, $4f^{13}$, and $4f^{12}$ inner sub-shell because, as was mentioned above, for preventing instability of the least-squares fits, similar parameters were varied simultaneously, keeping their ratios fixed and equal to the corresponding ratios of their Hartree-Fock values. Figure 7 shows the scaling factors for spin-orbit parameters, which are connected by similar ratios for all even configurations. It is seen that all scaling factors within the limits of the definition errors behave regularly and can be approximated by a straight line or a polynomial of second degree.

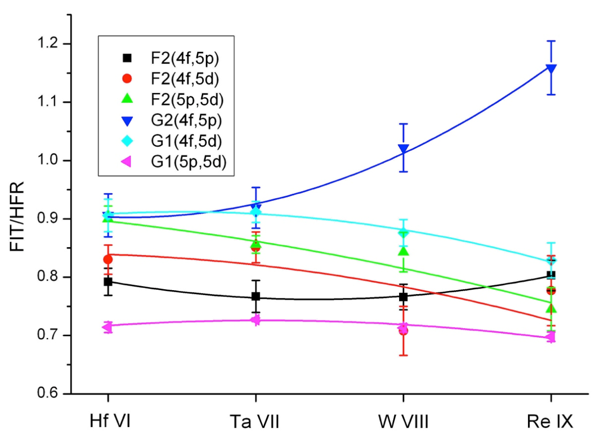

Figure 5. Scaling factors (ratios FIT/HFR) for main electrostatic parameters in the $4f^{13}5p^5nl$ and $4f^{14}5p^4nl$ configurations.

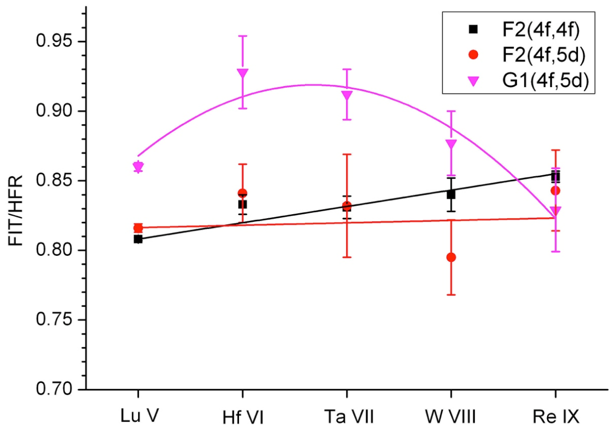

Figure 6. Scaling factors for main electrostatic parameters in the $4f^{12}5p^65d$ configuration.

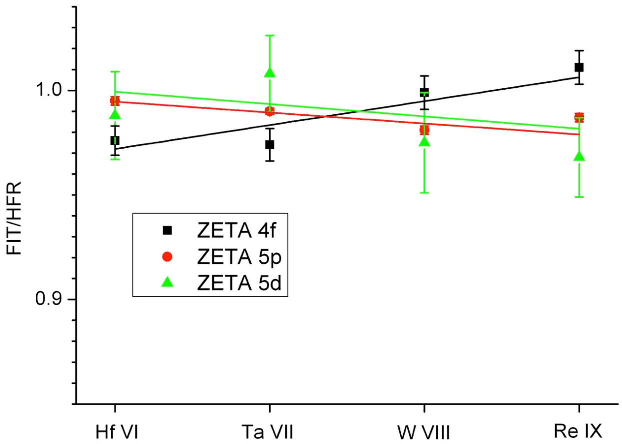

Figure 7. Scaling factors for spin-orbit parameters (ZETA) in the even configurations.

3.2. Spectrum of the W^{8+} Ion (W IX)

On the experimental spectrum recorded for the W VIII study (see Figure 3), a group of previously unidentified lines (marked by red colour) was observed between 170 Å and 200 Å, which could be due to W IX emission. It was possible to select lines that might belong to the W IX spectrum by measuring the variation of their intensities according to the plasma conditions. In the isoelectronic sequence of W IX, the last known members were Tm IV [24] and Yb V [25]. A systematic evaluation of energy ranges of low configurations along the isoelectronic sequence from Er III to W IX was given in Figure 2 of reference [25]. It predicted a change of the ground configuration from $4f^{12}5s^25p^6$ (Er III–Hf VII) to $4f^{14}5s^25p^4$ (Ta VIII and W IX).

Figure 8 shows a detailed structure of energy levels belonging to the $4f^{12}5s^25p^6$ configuration from Er III to Re IX. It was derived from calculations for the group of even configurations $4f^{12}5s^25p^6$ + $4f^{13}5s^25p^5$ + $4f^{14}5s^25p^4$, where all the HFR electrostatic integrals were scaled by a factor of 0.85 and the spin-orbit parameters were unscaled. The average energy E_{av} ($5s^25p^64f^{12}$) was set to zero for all the spectra, which explains the negative energies for many levels on the figure. The highest level of the $4f^{12}5s^25p^6$ configuration has a zero total angular momentum (J = 0), showing a $^1S_0$–$^3P_0$ mixing that increases with the increasing importance of the spin-orbit parameter ζ_{4f} relative to the Slater integrals F^k (4f,4f). Irregularity in its relative position along the isoelectronic sequence is a consequence of configuration interaction (CI) resulting from the crossing with the $4f^{14}5s^25p^4$ configuration, which has a downward trend from Er III to W IX as shown in Figure 2 of Reference [25]. Indeed, the other nearby even configuration $4f^{13}5s^25p^5$ has no level of J = 0 and produces CI effects only for levels of J = 1–4. The two J = 0 levels in the $4f^{14}5s^25p^4$ configuration have calculated energies of 55634 and 211895 cm^{-1} in Ta VIII, −68449 and 112556 cm^{-1} in W IX, −206333 and −7437 cm^{-1} in Re X. The resulting CI energy shifts on the highest J = 0 levels of the $4f^{12}5s^25p^6$ configurations in these ions are −3158, −4312, and +1682 cm^{-1}, respectively. This simple case shows the order of magnitude of possible CI shifts for all perturbed levels with other J values. Although this case is of limited practical interest as no strong transitions are involved, it illustrates a complexity that is even higher in the odd parity configurations in the W IX isoelectronic sequence.

Therefore, the structure of W IX is significantly more complex than in W VIII. Figure 9 shows the presently predicted structure of the W IX low-lying configurations, in which the ground configuration is $4f^{14}5s^25p^4$, and the $4f^{12}5s^25p^6$ configuration is even higher than the first excited configuration $4f^{13}5s^25p^5$. These three low-lying, even configurations result in three corresponding systems of excitations and E1 allowed transitions. Strongly interacting odd, excited configurations are all overlapping in the approximate energy range of 300,000 to 800,000 cm^{-1} above the ground state, which makes the predictions of the W IX spectrum critically dependent on the estimation of relative positions for energy levels. Figure 10 compares the W IX spectrum calculated in two approximations. In the approximation of Figure 10a the *ab initio* Hartree-Fock calculations were improved by a “standard” scaling of the energy parameters: scaling factors 0.85 for all electrostatic parameters and no scaling for spin-orbit parameters. The results in Figure 10b were obtained using the scaling factors from W VIII [10], which were derived from experimental levels (Table 3). Although these values do not significantly differ from the “standard” scaling factors, they nevertheless lead to drastic changes in the calculated spectra in the positions as well as in the intensities of the lines.

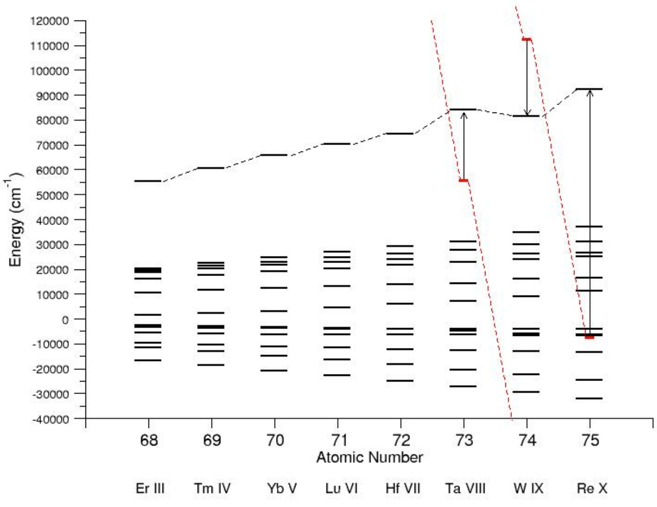

Figure 8. Isoelectronic comparison of the energy levels belonging to the $4f^{12}5s^25p^6$ configuration from Er III to Re IX (black bars). Black dashed lines trace the highest J = 0 level. Red dashed lines show the trend of changes for the two perturbing J = 0 levels of $4f^{14}5s^25p^4$. Only one J = 0 perturber could be represented (short red bars) on the chosen scale. Their perturbation effects are indicated by vertical arrows.

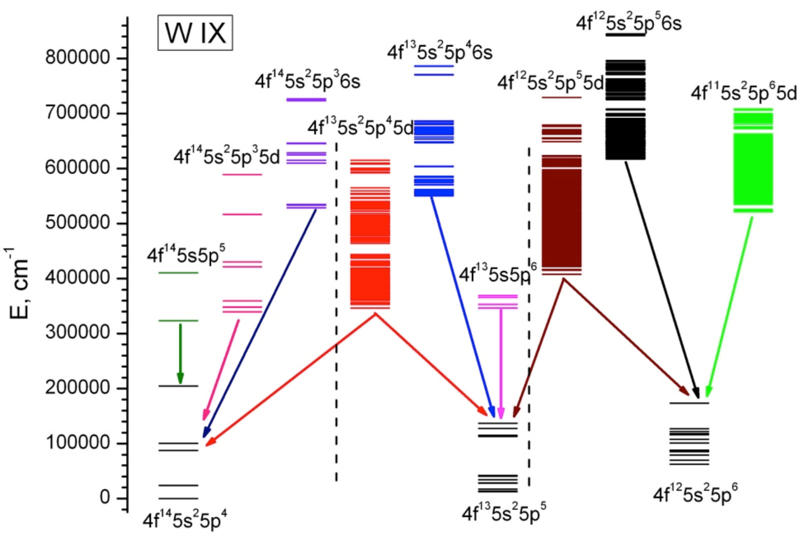

Figure 9. Low-lying energy levels of W IX according to Hartree-Fock calculations. Dashed vertical lines divide systems formed by excitation of the three lowest configurations: $4f^{14}5s^25p^4$, $4f^{13}5s^25p^5$, and $4f^{12}5s^25p^6$. Arrows indicate electric dipole transitions between the configurations.

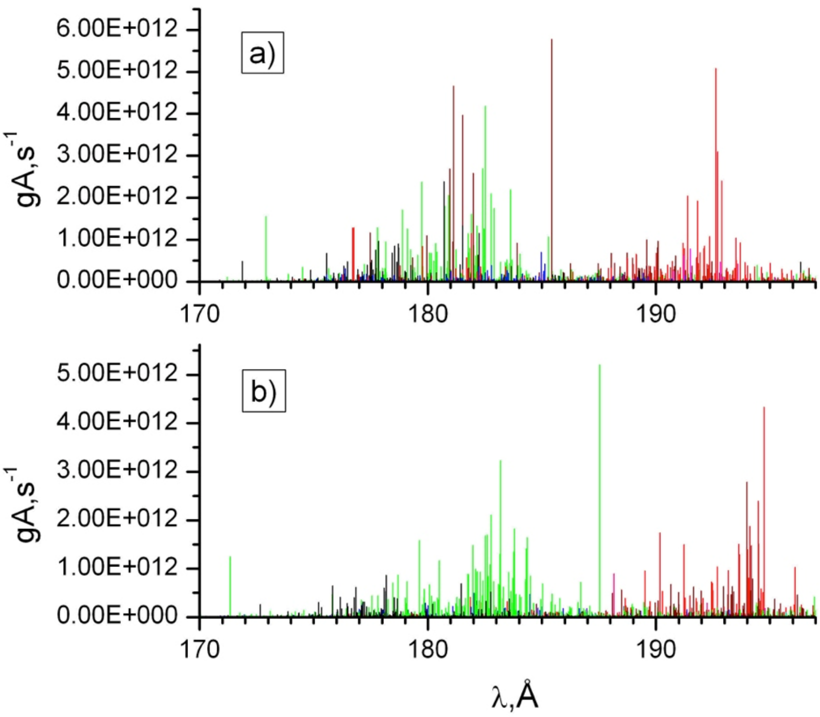

Figure 10. Calculated W IX spectrum: (**a**) "standard" scaling of Hartree-Fock parameters; (**b**) the Hartree-Fock parameters are scaled by the scaling factors taken from the W VIII spectrum. The colours of calculated lines correspond to the colours of transitions in Figure 9.

A list of the 189 strongest observed lines with intensities in the range of 50–1000, which could belong to W IX, is given in Table 4 (the full list consists of 483 spectral lines, see table S1 in Supplementary Materials). The wavelengths have an estimated uncertainty ±0.005 Å. The intensities of the lines are given in the same relative scale without correction for response of recording. It is impossible to reliably identify the W IX spectrum with the present predictions. More work is needed in the analyses of the isoelectronic spectra of the neighbouring chemical elements for making better calculations of the W IX spectrum. At this stage, it is only reasonable to suggest that the line at 193.830 Å can belong to the $4f^{13}5p^5\ ^3G_6$–$4f^{13}5p^45d\ (^3P)\ ^3H_6$ transition.

Table 4. Lines of W IX excited in a vacuum spark with intensities greater than 50 [a].

Int [a]	λ (Å)	σ(cm^{-1})
63	170.006	588215.3
84	170.203	587535.1
120	170.269	587306.0
339	170.336	587076.3
95	170.353	587017.1
120	170.648	586001.9
95	171.216	584056.2
309	172.038	581265.3
79	174.997	571437.4
56	175.490	569834.3
59	176.002	568174.1
81	176.493	566595.7
63	176.660	566060.4
82	176.752	565763.8
69	177.197	564342.1
102	177.468	563483.1
178	177.504	563367.9
66	177.591	563092.9
54	178.005	561782.3
97	178.115	561435.0
95	178.140	561355.3
67	178.220	561104.9
76	178.473	560308.2
104	178.490	560256.4
64	178.508	560199.6
86	178.956	558797.5
59	179.023	558588.7
110	179.631	556696.2
56	180.080	555310.0
69	180.164	555049.6
94	180.570	553802.8
109	180.922	552725.6
71	180.955	552624.8
128	180.986	552529.6
61	181.247	551733.3
51	181.428	551184.1
115	181.818	550000.3

Table 4. *Cont.*

Int [a]	λ (Å)	σ(cm^{-1})
100	181.835	549949.1
69	181.958	549578.9
74	182.184	548896.8
72	182.437	548135.0
143	182.505	547928.7
76	182.614	547604.1
77	182.824	546973.6
54	182.932	546652.4
166	182.990	546478.9
156	183.081	546205.8
107	183.093	546169.9
110	183.271	545640.7
53	183.305	545537.9
54	183.573	544743.0
51	183.771	544154.0
110	184.033	543380.8
63	184.070	543271.6
64	184.156	543018.2
248	184.200	542887.0
117	184.271	542680.2
58	184.438	542188.2
86	184.538	541893.8
95	184.545	541872.9
56	184.818	541072.3
59	185.727	538424.7
67	186.218	537004.4
54	186.297	536778.4
252	186.428	536399.6
51	186.456	536318.4
74	186.479	536253.7
79	186.506	536175.2
71	186.539	536080.1
166	186.680	535676.3
51	187.890	532225.4
92	188.104	531621.1
77	188.114	531591.4
104	188.197	531357.6
105	188.706	529925.1
82	189.264	528363.3
161	190.062	526143.6
66	190.391	525234.9
56	190.596	524670.6

Table 4. *Cont.*

Int [a]	λ (Å)	σ(cm^{-1})
107	191.103	523278.3
82	191.464	522291.7
304	191.933	521016.0
243	191.984	520876.5
54	192.090	520589.6
84	192.117	520516.2
87	192.468	519567.4
370	192.591	519234.0
199	192.715	518901.5
102	192.771	518749.7
541	192.834	518581.8
194	192.859	518514.3
132	193.091	517889.5
87	193.174	517667.5
115	193.229	517519.6
53	193.342	517218.7
118	193.411	517032.3
95	193.428	516987.7
290	193.490	516822.8
443	193.549	516664.0
303	193.636	516432.4
209	193.719	516210.8
181	193.771	516073.6
696	193.830	515915.8
362	193.999	515467.9
408	194.105	515184.6
148	194.140	515091.1
245	194.173	515006.0
229	194.201	514930.2
58	194.268	514752.3
500	194.355	514522.1
94	194.553	513998.2
1000	194.646	513752.1
66	194.792	513368.4
99	194.803	513339.9
77	194.832	513262.7
84	194.910	513057.8
66	195.114	512520.6
130	195.192	512315.8
153	195.259	512141.3
255	195.432	511685.6
102	195.469	511590.1
51	195.483	511552.7

Table 4. *Cont.*

Int [a]	λ (Å)	σ(cm^{-1})
439	195.679	511040.5
66	195.745	510869.3
67	195.794	510741.2
77	195.921	510410.6
140	196.129	509869.5
51	196.242	509573.9
53	196.371	509239.9
99	196.577	508707.6
192	196.592	508667.4
61	196.665	508478.4
66	196.732	508306.8
51	196.947	507751.1
357	196.966	507702.1
77	197.013	507579.9
120	197.057	507467.9
138	197.136	507263.3
169	197.350	506714.7
311	197.607	506056.2
72	197.736	505724.8
110	197.810	505535.9
66	198.008	505031.4
53	198.095	504807.3
114	198.196	504551.3
53	198.378	504088.7
71	198.391	504056.4
64	198.464	503869.7
128	198.543	503668.5
161	198.562	503621.8

[a] Relative intensity in arbitrary units not corrected for response of recording.

4. Conclusions

This work extended the state of knowledge on spectra of tungsten ions relevant for fusion plasma diagnostics. Using the spectrum of tungsten recorded on high resolution vacuum spectrographs under excitation in vacuum spark sources, a total of 187 lines of W VIII in the region 160–271 Å were identified for the first time. One hundred and two levels were found and transition probabilities were calculated [9,10]. For confirmation of the identifications of a spectrum as complex as W VIII, the isoelectronic spectra of neighboring chemical elements Hf VI, Ta VII, and Re IX were studied [11–13]. In each of these spectra, the transitions from $4f^{14}5s^25p^4nl$ and $4f^{13}5s^25p^6nl$ configurations to the low-lying configurations $4f^{14}5s^25p^5$ and $4f^{13}5s^25p^6$ were analyzed and, respectively 146, 130, and 87 energy levels were found. Previous analysis of Lu V [20] was extended by 22 newly identified lines and seven new levels. Parametric calculations of the spectra were performed with the aid of the Cowan codes [18], leading to fitted energy parameters together with their ratios to the corresponding *ab initio* values (scaling factors). In spite of sharp changes in relative positions of strongly interacting configurations along the isoelectronic sequence, resulting in noticeable variation in intensities and relative positions of lines, the scaling factors for the energy parameters show a rather regular trend. These isoelectronic regularities of scaling factors along the sequence Lu V – Hf VI – Ta VII – W VIII – Re IX can be considered as a proof of reliability of our atomic data for W VIII. Furthermore, the set of consistent scaling factors could be useful for predictions of other spectra of the 5d elements.

A list of 483 spectral lines in the region 170–199 Å, considered to belong to W IX, was prepared. The current state of the theory of atomic spectra does not allow for calculation of W IX with the accuracy needed for detailed identification of this spectrum and its application for quantitative diagnostics of tokamak plasmas.

Spectral lines from moderately charged tungsten ions (W IV–VI), in particular the 6p–6d and 6p–7s transitions of W V and the transitions between known levels of W III and W IV not reported in the compilation [2], are also present on our spectrograms. Their analyses are currently in progress.

Supplementary Materials

Table S1. Lines of W IX excited in a vacuum spark

Acknowledgments

This work was partly supported by the RFBR grant 10-02-00390a, by the Russian Academy of Sciences, by the French state funds managed by the Agence Nationale de Recherche (ANR) within the Investissements d'Avenir programme under reference ANR-11-IDEX-0004-02, and by a PPF grant of the Université Pierre et Marie Curie (UPMC). It is a part of the IAEA Coordinated Research Project "Spectroscopic and Collisional Data for Tungsten from 1 eV to 20 keV". One of us (JFW) is indebted to his late colleagues Victor Kaufman and Jack Sugar from the National Institute of Standards and Technology (USA) for communication of the wavelengths of the lutetium spark spectrum.

Author Contributions

All authors contributed equally to this work.

Conflicts of Interest

The authors declare no conflict of interest.

References

1. Skinner, C.H. Atomic physics in the quest for fusion energy and ITER. *Phys. Scr.* **2009**, *134*, 014022.
2. Kramida, A.E.; Shirai, T. Energy levels and spectral lines of tungsten, W III through W LXXIV. *At. Data Nucl. Data Tables* **2009**, *95*, 305–474.
3. Kramida, A.E. Recent progress in spectroscopy of tungsten. *Can. J. Phys*. **2011**, *89*, 551–570.
4. Veres, G.; Bakos, J.S.; Kardon, B. Energy levels and vacuum ultraviolet spectrum of W VIII. *J. Quant. Spectrosc. Ra.* **1996**, *56*, 295–301.

5. Sugar, J.; Kaufman, V. Seventh spectrum of tungsten (W VII); resonance lines of Hf V. *Phys. Rev. A* **1975**, *12*, 994–1012.
6. Clementson, J.; Beiersdorfer, P.; Magee, E.W.; McLean, H.S.; Wood, R.D. Tungsten spectroscopy relevant to the diagnostics of ITER divertor plasmas. *J. Phys. B* **2010**, *43*, 144009.
7. Suzuki, C.; Harte, C.S.; Kilbane, D.; Kato, T.; Sakaue, H.A.; Murakami, I.; Kato, D.; Sato, K.; Tamura, N.; Sudo, S.; *et al*. Interpretation of spectral emission in the 20 nm region from tungsten ions observed in fusion device plasmas. *J. Phys. B* **2011**, *44*, 175004.
8. International Atomic Energy Agency, Atomic Molecular Data Services. Available online: http://www-amdis.iaea.org/CRP/Tungsten/ (accessed on 1 April 2015).
9. Ryabtsev, A.N.; Kononov, E.Y.; Kildiyarova, R.R.; Tchang-Brillet, W.-Ü.L.; Wyart, J.-F. $4f^{13}5s^25p^6$–$4f^{13}5s^25p^56s$ Transitions in the W VIII spectrum and spectra of isoelectronic Hafnium, Tantalum, and Rhenium ions. *Opt. Spectrosc.* **2012**, *113*, 109–114.
10. Ryabtsev, A.N.; Kononov, E.Y.; Kildiyarova, R.R.; Tchang-Brillet, W.-Ü.L.; Wyart, J.-F. The spectrum of seven times ionized tungsten (W VIII) relevant to tokamak divertor plasmas. *Phys. Scr.* **2013**, *87*, 045303.
11. Ryabtsev, A.N.; Kononov, E.Y.; Kildiyarova, R.R.; Tchang-Brillet, W.-Ü.L.; Wyart, J.-F.; Champion, N.; Blaess, C. Spectra of the W VIII isoelectronic sequence: I. Hf VI. *Phys. Scr.* **2014**, *89*, 115402.
12. Ryabtsev, A.N.; Kononov, E.Y.; Kildiyarova, R.R.; Tchang-Brillet, W.-Ü.L.; Wyart, J.-F.; Champion, N.; Blaess, C. Spectra of the W VIII isoelectronic sequence: II.Ta VII. *Phys. Scr.* **2014**, *89*, 125403.
13. Ryabtsev, A.N.; Kononov, E.Y.; Kildiyarova, R.R.; Tchang-Brillet, W.-Ü.L.; Wyart, J.-F.; Champion, N.; Blaess, C. Spectra of the W VIII isoelectronic sequence: III. Re IX. *Phys. Scr.* **2015**, submitted.
14. Svensson, L.A.; Ekberg, J.O. The titanium vacuum-spark spectrum from 50 to 425 Å. *Ark. Fys.* **1969**, *40*, 145–164.
15. Engström, L. *Lund Reports on Atomic Physics, LRAP-232* (Lund, 1998). Available online: http://kurslab-atom.fysik.lth.se/Lars/Gfit/html/index.html (accessed on 17 June 2015).
16. Meftah, A.; Wyart, J.-F.; Sinzelle, J.; Tchang-Brillet, W.-Ü.L.; Champion, N.; Spector, N.; Sugar, J. Spectrum and energy levels of the Nd^{4+} free ion (Nd V). *Phys. Scr.* **2008**, *77*, 055302.
17. Azarov, V.I. Formal approach to the solution of the complex-spectra identification problem. 2. Implementaton. *Phys. Scr.* **1993**, *48*, 656–667.
18. Cowan, R.D. *The Theory of Atomic Structure and Spectra*; University of California Press: Berkeley, CA, USA, 1981.
19. Kramida, A.E. The program LOPT for least-squares optimization of energy levels. *Comput. Phys. Commun.* **2010**, *182*, 419–434.
20. Kaufman, V.; Sugar, J. Analysis of the spectrum of four-times-ionized lutetium (Lu V). *J. Opt. Soc. Am.* **1978**, *68*, 1529–1541.
21. Kaufman, V.; Sugar, J. National Institute of Standards and Technology, MD, USA. Unpublished line list, 1980.
22. Wyart, J.-F.; Kaufman, V.; Sugar, J. The $4f^{13}5f$ Configuration in the Isoelectronic Sequence of Yb III. *Phys. Scr.* **1981**, *23*, 1069–1078.

23. Wyart, J.-F.; Tchang-Brillet, W.-Ü.L.; Spector, N.; Palmeri, P.; Quinet, P.; Biemont, E. Extended analysis of the spectrum of triply-ionized ytterbium (Yb IV) and transition probabilities. *Phys. Scr.* **2001**, *63*, 113–121.
24. Meftah, A.; Wyart, J.-F.; Champion, N.; Tchang-Brillet, W.-Ü.L. Observation and interpretation of the Tm^{3+} free ion spectrum. *Eur. Phys. J. D* **2007**, *44*, 35–45.
25. Meftah, A.; Wyart, J.-F.; Tchang-Brillet, W.-Ü.L.; Blaess, C.; Champion, N. Spectrum and energy levels of the Yb^{4+} free ion (Yb V). *Phys. Scr.* **2013**, *88*, 045305.